Microscopic Modeling of Pump-Probe Spectroscopy and Population Inversion in Transition Metal Dichalcogenides

physica status solidi pss b
www.pss-b.com

Microscopic Modeling of Pump–Probe Spectroscopy and Population Inversion in Transition Metal Dichalcogenides

Raül Perea-Causín, Samuel Brem, and Ermin Malic*

Optical properties of transition metal dichalcogenide (TMD) monolayers are dominated by excitonic effects. These are significantly altered at high carrier densities, leading to energy renormalization, absorption bleaching, and even optical gain. Such effects are experimentally accessible in ultra-fast pump–probe measurements. Herein, the semiconductor Bloch equations are combined with the generalized Wannier equation to investigate the effect that excited carriers have on the excitonic properties of TMD monolayers. In particular, the dynamics of carrier occupation, energy renormalization, and absorption bleaching as well as population inversion and optical gain are investigated.

1. Introduction

Transition metal dichalcogenides (TMDs) have received much attention in the past years.[1–3] Formed by a layer of transition metal atoms (Mo, W) sandwiched between two layers of chalcogen atoms (S, Se), these materials are effectively 2D. A direct consequence is a strongly reduced screening, giving rise to an efficient Coulomb interaction and strongly bound excitons.[4–8] The importance of excitonic effects in TMDs is best seen in their optical spectra, which are dominated by the 1s exciton state and significantly enhanced with respect to free-particle spectra.[5,9] However, due to its excitonic nature, the optical response can significantly vary with increasing carrier density due to many-particle dielectric screening and Pauli blocking.[10] Therefore, carrier dynamics is accessible by measuring changes in optical spectra in pump–probe experiments.[11,12]

Previous pump–probe measurements have among others illustrated bandgap renormalization,[13,14] optical gain,[15] carrier thermalization,[16,17] and hot-phonon effects.[18] Recent theoretical studies have focused on stationary modeling of band renormalization,[10,19,20] absorption bleaching,[10] and optical gain.[21] To better connect theory and experiment, it is necessary to model the dynamics of charge carriers and resolve ultra-fast features in time, as most experiments use ultra-short femtosecond laser pulses, giving rise to nontrivial dynamics at strong excitations. In previous works we have performed microscopic calculations of pump–probe experiments in graphene,[22–25] where excitons do not play a significant role. More recently, we have also modeled exciton relaxation dynamics in TMDs[26,27] limited to weak excitations. Here, we apply the semiconductor Bloch equation (SBE) approach to investigate the dynamics of pump–probe experiments in TMDs at high excitation power. In particular, we temporally resolve the emergence of many-particle phenomena, such as population inversion, optical gain, bandgap renormalization and absorption bleaching.

R. Perea-Causín, S. Brem, E. Malic
Department of Physics
Chalmers University of Technology
412 96 Gothenburg, Sweden
E-mail: causin@chalmers.se

The ORCID identification number(s) for the author(s) of this article can be found under https://doi.org/10.1002/pssb.202000223.

DOI: 10.1002/pssb.202000223

2. Theory

We combine the SBEs with the generalized Wannier equation.[28,29] While the first describes the dynamics of charge carriers and the microscopic polarization, the second gives access to excitonic wavefunctions and excitonic binding energies. This information is exploited in the generalized Elliot formula to calculate the optical absorption as a function of carrier density. To resolve the carrier dynamics, we use the density matrix approach.[28,30,31] In this approach, the carrier occupation $f_{\mathbf{k}}^{\lambda} = \langle a_{\mathbf{k}}^{\lambda\dagger} a_{\mathbf{k}}^{\lambda} \rangle$ and the microscopic polarization $p_{\mathbf{k}} = \langle a_{\mathbf{k}}^{h} a_{\mathbf{k}}^{e} \rangle$ can be defined in terms of creation and annihilation operators $a_{\mathbf{k}}^{\lambda\dagger}$ and $a_{\mathbf{k}}^{\lambda}$ for electrons and holes ($\lambda = h, e$) with the momentum $\mathbf{k}$. We consider a many-particle Hamilton operator accounting for carrier–light, carrier–carrier, and carrier–phonon interactions.[30] The equations of motion for $f_{\mathbf{k}}^{\lambda}$ and $p_{\mathbf{k}}$ can then be obtained by making use of the Heisenberg equation. For the carrier–carrier interaction we stay at the Hartree–Fock level in the correlation expansion including formation of excitons.[32] Note that the inclusion of higher-order terms would lead to a linewidth broadening via excitation-induced dephasing[10,29] and may result in the appearance of trion and biexciton resonances in the optical spectra.[33,34] On the other hand, for the carrier–phonon interaction we go to the second-order Born–Markov approximation neglecting excitonic terms.

The resulting equations of motion are the well-known SBEs[28–31,35]

$$\dot{p}_{\mathbf{k}} = -i(\tilde{\omega}_{\mathbf{k}} - i\gamma_{\mathbf{k}})p_{\mathbf{k}} + i(1 - f_{\mathbf{k}}^{e} - f_{\mathbf{k}}^{h})\tilde{\Omega}_{\mathbf{k}} \tag{1}$$

$$\dot{f}_{\mathbf{k}}^{\lambda} = 2\Im\{\tilde{\Omega}_{\mathbf{k}}^{*} p_{\mathbf{k}}\} + \Gamma_{\mathbf{k}}^{\lambda,\mathrm{in}}(1 - f_{\mathbf{k}}^{\lambda}) - \Gamma_{\mathbf{k}}^{\lambda,\mathrm{out}} f_{\mathbf{k}}^{\lambda} - \gamma_{\mathrm{d}} f_{\mathbf{k}}^{\lambda} \tag{2}$$

Here, we have defined the Coulomb-renormalized energy as $\hbar\tilde{\omega}_{\mathbf{k}} = \hbar\omega_{\mathbf{k}} - \Sigma^{\mathrm{CH}} - \Sigma^{\mathrm{SX}}_{\mathbf{k}}$ with the zero-density band structure $\hbar\omega_{\mathbf{k}} = \varepsilon^h_{\mathbf{k}} + \varepsilon^e_{\mathbf{k}}$, the Coulomb-hole self energy $\Sigma^{\mathrm{CH}} = \sum_{\mathbf{q}}(V_{\mathbf{q}} - W_{\mathbf{q}})$, and the screened-exchange energy $\Sigma^{\mathrm{SX}}_{\mathbf{k}} = \sum_{\mathbf{k}'} W_{\mathbf{k}'-\mathbf{k}}(f^e_{\mathbf{k}'} + f^h_{\mathbf{k}'})$. We denote the unscreened Coulomb matrix element with $V_{\mathbf{q}}$, whereas $W_{\mathbf{q}}$ includes the dynamic screening computed according to the Lindhard formula.[30,36] We model the Coulomb interaction statically screened by the dielectric suroundings with the Rytova–Keldysh potential.[8,36–38] We have also defined the renormalized Rabi frequency as $\hbar\tilde{\Omega}_{\mathbf{k}} = i\frac{e_0}{m_0}\boldsymbol{M}_{\mathbf{k}} \cdot \boldsymbol{A}(t) + \sum_{\mathbf{k}'} W_{\mathbf{k}'-\mathbf{k}} p_{\mathbf{k}'}$, where $\boldsymbol{M}_{\mathbf{k}} = \langle \psi^c_{\mathbf{k}} | \hbar\mathbf{k} | \psi^v_{\mathbf{k}} \rangle$ is the optical matrix[32] element for interband transitions and $\boldsymbol{A}(t)$ is the time-dependent vector potential of the incident light pulse. The matrix element in the vicinity of the K point reads $|\boldsymbol{M}_{\mathbf{k}} \cdot \mathbf{e}_\sigma| = \frac{m_0}{\sqrt{2}}(1+\sigma)\sqrt{\frac{\varepsilon_g}{m_h + m_e}}$, where $\sigma = \pm 1$ for left (right) circular polarization of the incident light.[8,39] The vector potential $\boldsymbol{A}$ is modeled with a Gaussian temporal profile centered at $t = 0$ and oscillating with the frequency ω. Its amplitude is set by the fluence of the pulse, which corresponds to the energy flux $I(t) = \frac{1}{2}\epsilon_0 nc\omega^2 |\boldsymbol{A}(t)|^2$ integrated over time. Moreover, carrier–phonon scattering enters into the dephasing rate $\gamma_{\mathbf{k}}$ and the scattering rates $\Gamma^{\lambda,\mathrm{in(out)}}_{\mathbf{k}}$, which are computed at each time step and result from the second-order Born–Markov approximation.[23] Finally, we have included a phenomenological decay time $\tau_{\mathrm{d}} = \gamma_{\mathrm{d}}^{-1} = 6\,\mathrm{ps}$[15] to account for nonradiative decay channels after optical excitation. Note that we disregarded the dynamics of phonons, which are expected to become important at high excitations, but their effects are expected to become significant on a timescale of tens of picoseconds,[18,40,41] which is much longer than the optical excitation in the order of hundreds of femtoseconds.

While the dynamics of the system is fully described by the SBEs, the linear response of the excited sytem to the probe pulse is accessible through generalized exciton wavefunctions and the corresponding Elliot formula.[28,29] In the case of finite carrier densities, the Wannier equation, determining the exciton binding energies and wavefunctions, exhibits left-hand and right-hand solutions $\phi^{\nu\mathrm{R/L}}_{\mathbf{k}}$. The generalized Wannier equation for the right-hand wavefunction $\phi^{\nu\mathrm{R}}_{\mathbf{k}}$ reads[28,29]

$$\tilde{\varepsilon}_{\mathbf{k}}\phi^{\nu\mathrm{R}}_{\mathbf{k}} - (1 - f^e_{\mathbf{k}} - f^h_{\mathbf{k}})\sum_{\mathbf{k}'} W_{\mathbf{k}'-\mathbf{k}}\phi^{\nu\mathrm{R}}_{\mathbf{k}'} = \varepsilon^\nu \phi^{\nu\mathrm{R}}_{\mathbf{k}} \tag{3}$$

where ε^ν is the exciton resonance energy. By expressing Equation (1) on the basis of exciton wavefunctions and making use of the Wannier Equation (3) we can calculate density-dependent optical absorption via a generalized Elliot formula[29]

$$\alpha(\omega) \propto \frac{|\boldsymbol{M}_\sigma|^2}{\omega}\sum_\nu \Im\left\{\frac{\sum_{\mathbf{k}}(1 - f^e_{\mathbf{k}} - f^h_{\mathbf{k}})\phi^{\nu\mathrm{L}*}_{\mathbf{k}}\sum_{\mathbf{k}}\phi^{\nu\mathrm{R}}_{\mathbf{k}}}{\hbar\omega - \varepsilon^\nu + i\gamma}\right\} \tag{4}$$

where σ refers to the polarization of the incident light.

In the high-excitation regime, many carriers are created, which translates into a high occupation of the electronic states in the minima of the bands. This high occupation has two main effects on the excitonic properties. 1) The phase-space filling factor $(1 - f^e_{\mathbf{k}} - f^h_{\mathbf{k}})$ approaches zero, thus bleaching the absorption and reducing the electron–hole interaction due to Pauli blocking. 2) Dielectric screening significantly reduces the strength of the Coulomb interaction. While the bleaching of the absorption is manifested in the numerator of the Elliot formula 4, the reduction of the electron–hole interaction enters into the second term of the Wannier Equation (3). Furthermore, a very strong optical excitation can even lead to a sign inversion of the phase-space filling factor, resulting in negative absorption or optical gain (Equation (4)) and an effective repulsive electron–hole interaction (Equation (3)).

For our calculations, we use ab initio input parameters for the electronic band structure[42] (effective masses and bandgap), dielectric properties,[43] and carrier-phonon scattering[44] (optical phonon energies, acoustic phonon velocity, and the corresponding deformation potentials). While our theory applies principally to all excitonic materials, we focus on the exemplary case of monolayer WS_2 on a SiO_2 substrate at room temperature. Note that a stronger dielectric screening (e.g., in the case of hBN encapsulation) will reduce the Coulomb interaction, resulting in a lower exciton binding energy, energy renormalization, and optical absorption. For the optical excitation, we consider a 200 fs pulse centered at the A exciton resonance (2 eV) with a fluence of 10 μJ cm^{-2}. Note that we do not consider any dark exciton states.[45–47]

3. Carrier Dynamics

We solve the SBEs numerically for the system described earlier and obtain the energy- and time-resolved carrier occupations. In the considered strong excitation regime and a pump energy of 2 eV, we obtain a peak carrier density of $3 \times 12\,\mathrm{cm}^{-2}$. We show the electron occupation in **Figure 1**, noting that the respective figure for holes is similar. We observe an ultra-fast creation of electrons at the timescale of the pulse duration (200 fs) with the occupation approaching 1 at small kinetic energies. This high occupation corresponds to a population inversion, i.e., a higher electron occupation in the conduction band than in the valence band. As will be shown later, this leads to a negative absorption or optical gain. It is noteworthy to mention that population inversion becomes less pronounced for longer pulses, as the slowly evolving distribution saturates to half filling, where the phase-space filling factor is zero. As we consider an excitation resonant to the 1s exciton, the momentum dependence of the carrier generation should have the shape of the excitonic ground-state wavefunction. However, the high carrier density results in a nontrivial temporal evolution of the carrier occupation. In fact, during the excitation we observe a pronounced spectral broadening of the carrier distribution (Figure 1b), which results from 1) Pauli blocking leading to a saturation of absorption at small momenta, whereas absorption still occurs at higher momenta and 2) carrier generation shifts to higher momenta as the bandgap shifts below the excitation energy (cf. **Figure 2**b). The distribution also exhibits a small peak at renormalized energy in resonance with optical excitation (e.g. 64 meV at $t = 0.2$ ps) and replicas of this peak due to scattering with optical phonons (cf. the peaks at 22 and 106 meV at $t = 0.2$ ps). After optical excitation, the electrons relax into a thermal distribution through scattering with phonons and the overall population decays on a timescale of a few picoseconds—corresponding to the phenomenological decay time.

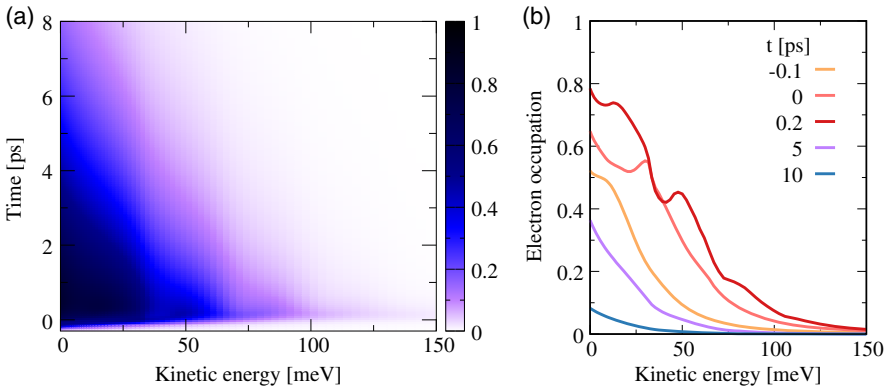

Figure 1. Time- and energy-resolved electron occupation. a) Color map of the electron occupation as a function of time and energy. b) Time cuts of the electron occupation as a function of energy.

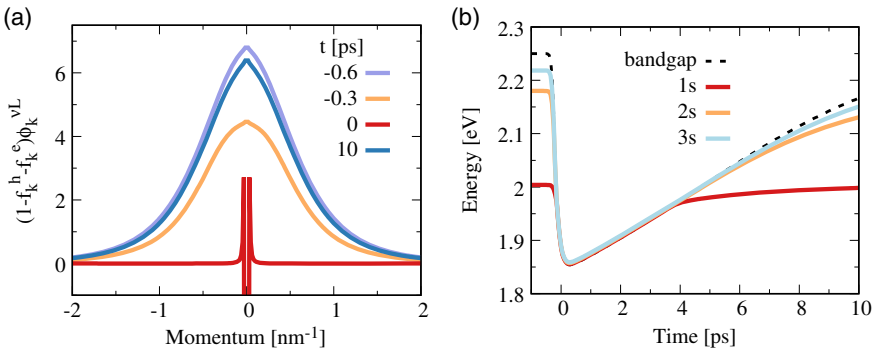

Figure 2. Time-resolved excitonic properties. a) Bleaching of the exciton wavefunction expressed by $(1-f_{\mathbf{k}}^{e}-f_{\mathbf{k}}^{h})\phi_{\mathbf{k}}^{\nu L}$ shown at different times. b) Renormalization of the single-particle bandgap and excitonic binding energies as a function of time.

4. Excitonic Properties

After solving the SBEs, we plug the time- and energy-resolved carrier occupations in the Wannier equation to obtain the time-resolved exciton wavefunctions and exciton binding energies (cf. Figure 2). When the pulse starts exciting carriers ($t = 0.3$ ps, Figure 2a), the bleaching/reduction of the wavefunctions due to Pauli blocking is already noticeable. At the center of the excitation pulse ($t = 0$ ps) the excitonic wavefunction resembles one of scattering states[48] (sharp oscillating profile) including negative regions. While the sign inversion is caused by population inversion, the sharp momentum profile is induced by a combination of many-particle dielectric screening and Pauli blocking and is characteristic of continuum (scattering) states. Note that an unbound electron–hole pair has a planewave as the wavefunction, corresponding to a sharp peak in momentum space. After 10 ps the carrier population mostly decays, resulting in the recovery of the zero-density excitonic properties.

In addition to the wavefunctions, a high carrier occupation affects the exciton binding energies as well as the single-particle bandgap. Figure 2b shows the temporal evolution of exciton energies and the single-particle bandgap. Before the pulse both quantities remain constant. Under strong pulse exciation, the bandgap undergoes a drastic red-shift of 400 meV—in agreement with previous experimental[15] and theoretical[20] studies. The exciton binding energies become smaller, approaching the value of the bandgap, where there are no bound states anymore. After the optical excitation, the bandgap and the exciton energies slowly recover their original values. Note that at sufficiently high carrier densities there are no excitonic bound states and the system is no longer dominated by bound electron–hole pairs but by an electron–hole plasma.[49] This Mott transition is reflected in the wavefunction of the 1s state resembling a scattering wavefunction at the center of the pulse (Figure 2a at $t = 0$ ps). We expect the Mott transition to occur at slightly higher densities when accounting for other electronic valleys and heating mechanisms.

5. Absorption Spectra

Optical absorption can be modeled by evaluating the Elliot formula (Equation (4)), where exciton wavefunctions and exciton resonance appear. Hence, the time-resolved wavefunctions and energies shown in Figure 2 can be used to calculate the temporal evolution of the optical absorption (cf. **Figure 3**a,b). We observe that excitonic features in the optical absorption are quickly bleached under the strong optical excitation. The 1s exciton peak at 2 eV undergoes first a red-shift and afterward apparently a blue-shift, as observed in previous studies.[19]

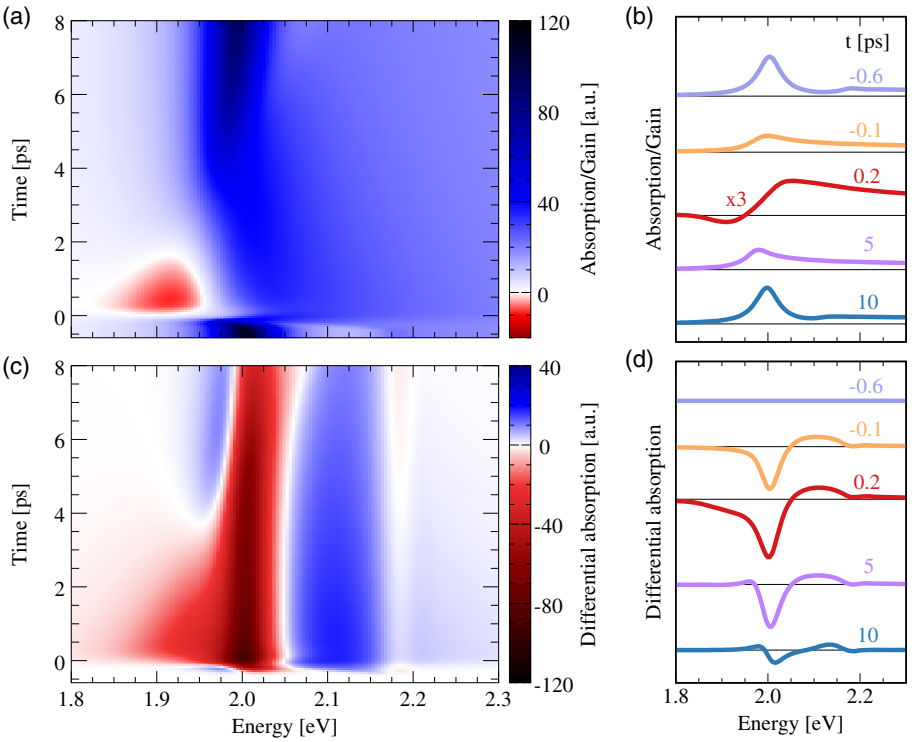

Figure 3. Time-resolved optical spectra. a,b) Color map and time cuts illustrating the optical absorption. The absorption at $t = 0.2$ ps is rescaled to highlight the optical gain. c,d) Color map and time cuts showing differential absorption.

While the first shift is directly related to the red-shift of the exciton resonance energy (cf. Figure 2b), the second shift is only a result of bleaching of the optical transition at the lowest energetic states caused by the high carrier population. The higher energy wing appears then as a blue-shift (cf. the 0.2 ps curve in Figure 3b). At the same time, the absorption intensity is considerably reduced due to phase-space filling, i.e., blocking of optical transitions, and bleached Coulomb interaction, resulting in a reduced excitonic enhancement (note that the 0.2 ps curve has been multiplied by a factor of 3). After optical excitation, the intrinsic optical properties of the material are restored as the carrier population decays and the exciton properties recover their initial values. For sufficiently large optical excitation even a carrier population inversion can be obtained. This results in a negative phase-space filling factor, which translates into negative absorption and hence optical gain (cf. the red-colored region in Figure 3a). This phenomenon has been already experimentally observed in the material studied here[15] and can become more prominent and spectrally broader at higher excitation densities.[50] We find that optical gain becomes less pronounced for longer pulse durations due to a lower population inversion and it is almost nonexistent for a 1.5 ps pulse (not shown here).

6. Differential Absorption

To experimentally investigate temporal changes in absorption spectra, differential absorption/transmission spectroscopy is often applied. Here, we track the variation of an optical spectrum at a given time with respect to the spectrum before optical excitation (cf. Figure 3c,d). Spectral shifts of resonances in absorption spectra can be traced by the appearance of zero crossings in differential absorption spectra, whereas efficient absorption bleaching can be identified by strong negative signals. We observe two zero crossings around 2.0 and 2.2.eV corresponding to the shifts of 1s and 2s exciton resonances (cf. Figure 3d and white areas in Figure 3c). Strongly pronounced negative differential absorption (red regions) is found around the 1s exciton energy reflecting an efficient absorption bleaching in this spectral range. The huge bandgap renormalization predicted in Figure 2b is manifested in the increased absorption between the 1 and 2s exciton energies (blue region in Figure 3c). Population inversion (optical gain) is reflected in a decreased absorption at energies below the 1s resonance energy, which corresponds to the bottom of the renormalized band (cf. Figure 2b). These results are consistent with experimental observations in similar materials.[13,15,19]

While we focus here on moderately strong excitation densities, much weaker excitations lead to changes in the absorption that are not visible with the naked eye (small energy shifts and bleaching) but that can be resolved with differential absorption. Furthermore, the effect of the excitation energy on the temporal evolution of optical spectra is nontrivial. To investigate this, we calculate the differential absorption at 1s resonance energy (2 eV) for different pump energies (**Figure 4**a) and different pump fluences (Figure 4b). We observe that the minimum of the differential absorption is delayed for pump energies above the bandgap with the delay time increasing for higher excitation

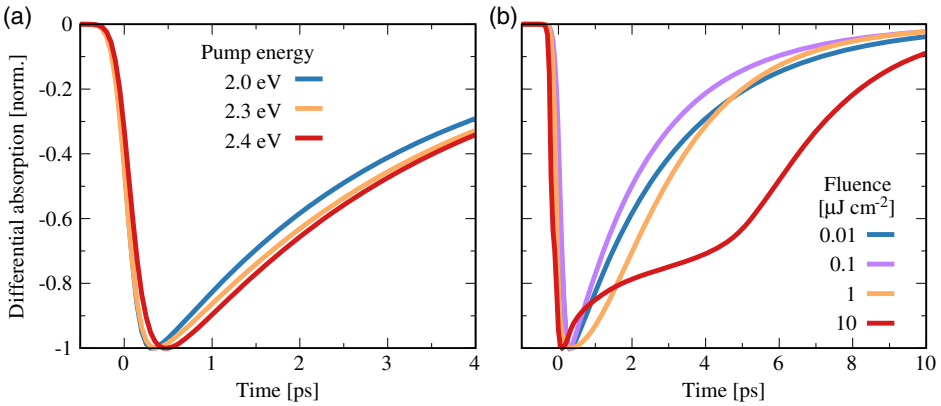

Figure 4. Time-resolved differential absorption at the probe energy 2 eV corresponding to the 1s resonance energy at zero density for a) different pump energies and a fixed pump fluence of 10 nJ cm^{-2} and b) varying pump fluences at a fixed pump energy of 2 eV. The results are normalized with respect to the peak of each curve to better illustrate the relative differences.

energies. The reason behind this behaviour is that the bleaching of the 1s peak in the optical absorption is less efficient when the carriers are not at the bottom of the bands. Hence, the bleaching is maximized only after the carriers have scattered to the lowest energetic states and the observed delay is thus a direct signature of carrier thermalization. Furthermore, we observe that the differential absorption decays and recovers faster for a fluence of 0.1 μJ cm^{-2} compared with the case for 0.01 μJ cm^{-2} (we observe the same trend at lower excitation densities). We identify this feature to be a result of the complex time dependence of absorption (Equation (4)). Note that this trend can be reproduced by assuming a Lorentzian profile (representing the 1s absorption peak) with an exponentially decaying small deviation from the resonance energy and the peak intensity. For an even higher fluence of 1 μJ cm^{-2}, the minimum extends over a longer time due to the saturation of absorption caused by Pauli blocking and then recovers at a similar rate as for lower fluences. Finally, for the case at 10 μJ cm^{-2}, we observe a fast initial recovery as a result of the enhanced carrier recombination which results from population inversion giving rise to stimulated emission. At later times, the recovery of differential absorption develops a plateau as a consequence of the complex interplay between the energy renormalization, absorption bleaching, and their nontrivial time evolution at elevated carrier densities. Note that this plateau spans during the time when the system is beyond the Mott transition (cf. Figure 2b where no clear bound states appear until $t = 4$–5 ps). The final recovery is similar to the one exhibited at lower fluences, when the system is far below the Mott transition. Note that a similar fast initial decay has been experimentally observed, although it was atributed to carrier thermalization and heating due to hot phonons.[17]

7. Conclusions

We have microscopically modeled pump–probe experiments at a high excitation power in TMDs disentangling the time evolution of carrier occupation, exciton wavefunction, exciton binding energies, electronic bandgap, and absorption spectra. Based on SBE, we have resolved the nontrivial carrier dynamics in the strong excitation regime, marked by a broadening of the carrier distribution caused by absorption saturation and bandgap renormalization. Moreover, by solving the Wannier equation we have provided access to the temporal evolution of excitonic properties, observing the Mott transition and a large energy renormalization. Finally, we have mapped the carrier and exciton dynamics into optical absorption spectra, monitoring the peak bleaching and energy shifts and even demonstrating the appearance of optical gain.

Acknowledgements

This project has received funding from the Swedish Research Council (VR, project number 2018-00734), the European Union's Horizon 2020 research and innovation programme under grant agreement no 881603 (Graphene Flagship), and Chalmers' Excellence Initiative Nano under its Excellence PhD programme.

Conflict of Interest

The authors declare no conflict of interest.

Keywords

carrier dynamics, excitons, strong excitation, transition metal dichalcogenides

Received: April 17, 2020
Revised: June 10, 2020
Published online:

[1] G. Wang, A. Chernikov, M. M. Glazov, T. F. Heinz, X. Marie, T. Amand, B. Urbaszek, *Rev. Mod. Phys.* **2018**, *90*, 021001.
[2] T. Mueller, E. Malic, *npj 2D Mater. Appl.* **2018**, *2*, 1.
[3] S. Manzeli, D. Ovchinnikov, D. Pasquier, O. V. Yazyev, A. Kis, *Nat. Rev. Mater.* **2017**, *2*, 17033.
[4] M. M. Ugeda, A. J. Bradley, S. F. Shi, H. Felipe, Y. Zhang, D. Y. Qiu, W. Ruan, S. K. Mo, Z. Hussain, Z. X. Shen, F. Wang, S. G. Louie, M. F. Crommie, *Nat. Mater.* **2014**, *13*, 1091.

[5] A. Chernikov, T. C. Berkelbach, H. M. Hill, A. Rigosi, Y. Li, O. B. Aslan, D. R. Reichman, M. S. Hybertsen, T. F. Heinz, *Phys. Rev. Lett.* **2014**, *113*, 076802.
[6] K. He, N. Kumar, L. Zhao, Z. Wang, K. F. Mak, H. Zhao, J. Shan, *Phys. Rev. Lett.* **2014**, *113*, 026803.
[7] A. Ramasubramaniam, *Phys. Rev. B* **2012**, *86*, 115409.
[8] G. Berghäuser, E. Malic, *Phys. Rev. B* **2014**, *89*, 125309.
[9] K. F. Mak, C. Lee, J. Hone, J. Shan, T. F. Heinz, *Phys. Rev. Lett.* **2010**, *105*, 136805.
[10] A. Steinhoff, M. Rosner, F. Jahnke, T. O. Wehling, C. Gies, *Nano Lett.* **2014**, *14*, 3743.
[11] R. Schmidt, G. Berghauser, R. Schneider, M. Selig, P. Tonndorf, E. Malic, A. Knorr, S. Michaelis de Vasconcellos, R. Bratschitsch, *Nano Lett.* **2016**, *16*, 2945.
[12] S. Sim, J. Park, J. G. Song, C. In, Y. S. Lee, H. Kim, H. Choi, *Phys. Rev. B* **2013**, *88*, 075434.
[13] E. A. Pogna, M. Marsili, D. De Fazio, S. Dal Conte, C. Manzoni, D. Sangalli, D. Yoon, A. Lombardo, A. C. Ferrari, A. Marini, G. Cerullo, D. Prezzi, *ACS Nano* **2016**, *10*, 1182.
[14] P. D. Cunningham, A. T. Hanbicki, K. M. McCreary, B. T. Jonker, *ACS Nano* **2017**, *11*, 12601.
[15] A. Chernikov, C. Ruppert, H. M. Hill, A. F. Rigosi, T. F. Heinz, *Nat. Photonics* **2015**, *9*, 466.
[16] F. Ceballos, Q. Cui, M. Z. Bellus, H. Zhao, *Nanoscale* **2016**, *8*, 11681.
[17] Z. Nie, R. Long, L. Sun, C. C. Huang, J. Zhang, Q. Xiong, D. W. Hewak, Z. Shen, O. V. Prezhdo,. H. Loh, *ACS Nano* **2014**, *8*, 10931.
[18] C. Ruppert, A. Chernikov, H. M. Hill, A. F. Rigosi, T. F. Heinz, *Nano Lett.* **2017**, *17*, 644.
[19] E. J. Sie, A. Steinhoff, C. Gies, C. H. Lui, Q. Ma, M. Rosner, G. Schönhoff, F. Jahnke, T. O. Wehling, Y. H. Lee, J. Kong, P. Jarillo-Herrero, N. Gedik, *Nano Lett.* **2017**, *17*, 4210.
[20] D. Erben, A. Steinhoff, C. Gies, G. Schönhoff, T. Wehling, F. Jahnke, *Phys. Rev. B* **2018**, *98*, 035434.
[21] L. Meckbach, T. Stroucken, S. W. Koch, *Appl. Phys. Lett.* **2018**, *112*, 061104.
[22] E. Malic, A. Knorr, *Graphene and Carbon Nanotubes: Ultrafast Optics and Relaxation Dynamics*, Wiley-VCH, Weinheim, Germany **2013**.
[23] E. Malic, T. Winzer, E. Bobkin, A. Knorr, *Phys. Rev. B* **2011**, *84*, 205406.
[24] S. Winnerl, M. Orlita, P. Plochocka, P. Kossacki, M. Potemski, T. Winzer, E. Malic, A. Knorr, M. Sprinkle, C. Berger, W. A. de Heer, H. Schneider, M. Helm, *Phys. Rev. Lett.* **2011**, *107*, 237401.
[25] F. Kadi, T. Winzer, E. Malic, A. Knorr, F. Göttfert, M. Mittendorff, S. Winnerl, M. Helm, *Phys. Rev. Lett.* **2014**, *113*, 035502.
[26] S. Brem, M. Selig, G. Berghaeuser, E. Malic, *Sci. Rep.* **2018**, *8*, 1.
[27] M. Selig, G. Berghäuser, M. Richter, R. Bratschitsch, A. Knorr, E. Malic, *2D Mater.* **2018**, *5*, 035017.
[28] M. Kira, S. W. Koch, *Prog. Quantum Electron.* **2006**, *30*, 155.
[29] M. Kira, S. W. Koch, *Semiconductor Quantum Optics*, Cambridge University Press, Cambridge, UK **2011**.
[30] H. Haug, S. W. Koch, *Quantum Theory of the Optical and Electronic Properties of Semiconductors: 5th Edition*, World Scientific Publishing Company, London, UK **2009**.
[31] F. Rossi, T. Kuhn, *Rev. Mod. Phys.* **2002**, *74*, 895.
[32] E. Malic, J. Maultzsch, S. Reich, A. Knorr, *Phys. Rev. B* **2010**, *82*, 115439.
[33] Z. Li, T. Wang, Z. Lu, C. Jin, Y. Chen, Y. Meng, Z. Lian, T. Taniguchi, K. Watanabe, S. Zhang, D. Smirnov, S.-F. Shi, *Nat. Commun.* **2018**, *9*, 1.
[34] A. Steinhoff, M. Florian, A. Singh, K. Tran, M. Kolarczik, S. Helmrich, A. W. Achtstein, U. Woggon, N. Owschimikow, F. Jahnke, X. Li, *Nat. Phys.* **2018**, *14*, 1199.
[35] M. Lindberg, S. W. Koch, *Phys. Rev. B* **1988**, *38*, 3342.
[36] B. Scharf, D. Van Tuan, I. Žutić, H. Dery, *J. Phys.: Condens. Matter* **2019**, *31*, 203001.
[37] N. S. Rytova, *Moscow Univ. Phys. Bull.* **1967**, *3*, 18.
[38] L. Keldysh, *Phys. Lett.* **1979**, *29*, 658.
[39] D. Xiao, G. B. Liu, W. Feng, X. Xu, W. Yao, *Phys. Rev. Lett.* **2012**, *108*, 196802.
[40] R. Perea-Causin, S. Brem, R. Rosati, R. Jago, M. Kulig, J. D. Ziegler, J. Zipfel, A. Chernikov, E. Malic, *Nano Lett.* **2019**, *19*, 7317.
[41] M. Glazov, *Phys. Rev. B* **2019**, *100*, 045426.
[42] A. Kormányos, G. Burkard, M. Gmitra, J. Fabian, V. Zólyomi, N. D. Drummond, V. Falko, *2D Mater.* **2015**, *2*, 022001.
[43] A. Laturia, M. L. Van de Put, W. G. Vandenberghe, *npj 2D Mater. Appl.* **2018**, *2*, 1.
[44] Z. Jin, X. Li, J. T. Mullen, K. W. Kim, *Phys. Rev. B* **2014**, *90*, 045422.
[45] M. Feierabend, G. Berghäuser, A. Knorr, E. Malic, *Nat. Commun.* **2017**, *8*, 1.
[46] E. Malic, M. Selig, M. Feierabend, S. Brem, D. Christiansen, F. Wendler, A. Knorr, G. Berghäuser, *Phys. Rev. Mater.* **2018**, *2*, 014002.
[47] S. Brem, A. Ekman, D. Christiansen, F. Katsch, M. Selig, C. Robert, X. Marie, B. Urbaszek, A. Knorr, E. Malic, *Nano Lett.* **2020**, *20*, 2849.
[48] L. Landau, E. Lifshitz, *Quantum Mechanics: Non-Relativistic Theory*, Course of Theoretical Physics, Vol. 3, Third edition, Pergamon, London, UK **1977**, pp. 102–132.
[49] A. Steinhoff, M. Florian, M. Rösner, G. Schönhoff, T. Wehling, F. Jahnke, *Nat. Commun.* **2017**, *8*, 1.
[50] F. Lohof, A. Steinhoff, M. Florian, M. Lorke, D. Erben, F. Jahnke, C. Gies, *Nano Lett.* **2018**, *19*, 210.